Article

A Highly Conserved Program of Neuronal Microexons Is Misregulated in Autistic Brains

Manuel Irimia,[1,2,*] Robert J. Weatheritt,[1,3] Jonathan D. Ellis,[1] Neelroop N. Parikshak,[4] Thomas Gonatopoulos-Pournatzis,[1] Mariana Babor,[1] Mathieu Quesnel-Vallières,[1] Javier Tapial,[2] Bushra Raj,[1] Dave O'Hanlon,[1] Miriam Barrios-Rodiles,[6] Michael J.E. Sternberg,[5] Sabine P. Cordes,[6,7] Frederick P. Roth,[1,6,7,8,9] Jeffrey L. Wrana,[6,7] Daniel H. Geschwind,[4] and Benjamin J. Blencowe[1,7,*]

[1]Donnelly Centre, University of Toronto, 160 College Street, Toronto, ON M5S 3E1, Canada
[2]EMBL/CRG Research Unit in Systems Biology, Centre for Genomic Regulation (CRG), 88 Dr. Aiguader, Barcelona 08003, Spain
[3]MRC Laboratory of Molecular Biology, Francis Crick Avenue, Cambridge CB2 0QH, UK
[4]Department of Neurology, Center for Autism Research and Treatment, Semel Institute, David Geffen School of Medicine, University of California Los Angeles, 695 Charles E. Young Drive South, Los Angeles, CA 90095, USA
[5]Centre for Integrative Systems Biology and Bioinformatics, Department of Life Sciences, Imperial College London, London SW7 2AZ, UK
[6]Lunenfeld-Tanenbaum Research Institute, Mount Sinai Hospital, 600 University Avenue, Toronto, ON M5G 1X5, Canada
[7]Department of Molecular Genetics, University of Toronto, 1 King's College Circle, Toronto, ON M5S 1A8, Canada
[8]Department of Computer Science, University of Toronto, 10 King's College Road, Toronto, ON M5S 3G4, Canada
[9]Canadian Institute For Advanced Research, 180 Dundas Street West, Toronto, ON M5G 1Z8, Canada
*Correspondence: mirimia@gmail.com (M.I.), b.blencowe@utoronto.ca (B.J.B.)
http://dx.doi.org/10.1016/j.cell.2014.11.035

SUMMARY

Alternative splicing (AS) generates vast transcriptomic and proteomic complexity. However, which of the myriad of detected AS events provide important biological functions is not well understood. Here, we define the largest program of functionally coordinated, neural-regulated AS described to date in mammals. Relative to all other types of AS within this program, 3-15 nucleotide "microexons" display the most striking evolutionary conservation and switch-like regulation. These microexons modulate the function of interaction domains of proteins involved in neurogenesis. Most neural microexons are regulated by the neuronal-specific splicing factor nSR100/SRRM4, through its binding to adjacent intronic enhancer motifs. Neural microexons are frequently misregulated in the brains of individuals with autism spectrum disorder, and this misregulation is associated with reduced levels of nSR100. The results thus reveal a highly conserved program of dynamic microexon regulation associated with the remodeling of protein-interaction networks during neurogenesis, the misregulation of which is linked to autism.

INTRODUCTION

Alternative splicing (AS)—the process by which different pairs of splice sites are selected in precursor mRNA to generate multiple mRNA and protein products—is responsible for greatly expanding the functional and regulatory capacity of metazoan genomes (Braunschweig et al., 2013; Chen and Manley, 2009; Kalsotra and Cooper, 2011). For example, transcripts from over 95% of human multiexon genes undergo AS, and most of the resulting mRNA splice variants are variably expressed between different cell and tissue types (Pan et al., 2008; Wang et al., 2008). However, the function of the vast majority of AS events detected to date are not known, and new landscapes of AS regulation remain to be discovered and characterized (Braunschweig et al., 2014; Eom et al., 2013). Moreover, because the misregulation of AS frequently causes or contributes to human disease, there is a pressing need to systematically define the functions of splice variants in disease contexts.

AS generates transcriptomic complexity through differential selection of cassette alternative exons, alternative 5′ and 3′ splice sites, mutually exclusive exons, and alternative intron retention. These events are regulated by the interplay of cis-acting motifs and trans-acting factors that control the assembly of spliceosomes (Chen and Manley, 2009; Wahl et al., 2009). The assembly of spliceosomes at 5′ and 3′ splice sites is typically regulated by RNA-binding proteins (RBPs) that recognize proximal cis-elements, referred to as exonic/intronic splicing enhancers and silencers (Chen and Manley, 2009). An important advance that is facilitating a more general understanding of the role of individual AS events is the observation that many cell/tissue type- and developmentally-regulated AS events are coordinately controlled by individual RBPs, and that these events are significantly enriched in genes that operate in common biological processes and pathways (Calarco et al., 2011; Irimia and Blencowe, 2012; Licatalosi and Darnell, 2010).

AS can have dramatic consequences on protein function and/or affect the expression, localization, and stability of spliced mRNAs (Irimia and Blencowe, 2012). Whereas cell and tissue differentially regulated AS events are significantly underrepresented in functionally defined, folded domains in proteins, they

are enriched in regions of protein disorder that typically are surface accessible and embed short linear interaction motifs (Buljan et al., 2012; Ellis et al., 2012; Romero et al., 2006). AS events located in these regions are predicted to participate in interactions with proteins and other ligands (Buljan et al., 2012; Weatheritt et al., 2012). Indeed, among a set of analyzed neural-specific exons enriched in disordered regions, approximately one-third promoted or disrupted interactions with partner proteins (Ellis et al., 2012). These observations suggested that a widespread role for regulated exons is to specify cell and tissue type-specific protein-interaction networks.

Human disease mutations often disrupt *cis*-elements that control splicing and result in aberrant AS patterns (Cartegni et al., 2002). Other disease changes affect the activity or expression of RBPs, causing entire programs of AS to be misregulated. For example, amyotrophic lateral sclerosis-causing mutations in the RBPs TLS/FUS and TDP43 affect AS and other aspects of posttranscriptional regulation (Polymenidou et al., 2012), and changes in the expression of the RBP RBFOX1 have been linked to misregulation of AS in the brains of individuals with autism spectrum disorder (ASD) (Voineagu et al., 2011). It is also widely established that misregulation of AS plays important roles in altering the growth and invasiveness of various cancers (David and Manley, 2010). As is the case with assessing the normal functions of AS, it is generally not known which disease-misregulated AS events cause or contribute to disease phenotypes.

Central to addressing the above questions is the importance of comprehensively defining AS programs associated with normal and disease biology. Gene-prediction algorithms, high-throughput RNA sequencing (RNA-seq) analysis methods, and RNA-seq data sets generally lack the sensitivity and/or depth required to detect specific types of AS. In particular, microexons (Beachy et al., 1985; Coleman et al., 1987), defined here as 3–27 nucleotide (nt)-long exons, have been largely missed by genome annotations and transcriptome profiling studies (Volfovsky et al., 2003; Wu et al., 2013; Wu and Watanabe, 2005). This is especially true for microexons shorter than 15 nt. Furthermore, where alignment tools have been developed to capture microexons (Wu et al., 2013), they have not been applied to the analysis of different cell and tissue types or disease states.

In this study, we developed an RNA-seq pipeline for the systematic discovery and analysis of all classes of AS, including microexons. By applying this pipeline to deep RNA-seq data sets from more than 50 diverse cell and tissue types, as well as developmental stages, from human and mouse, we define a large program of neural-regulated AS. Strikingly, neural-included microexons represent the most highly conserved and dynamically regulated component of this program, and the corresponding genes are highly enriched in neuronal functions. These microexons are enriched on the surfaces of protein-interaction domains and are under strong selection pressure to preserve reading frame. We also observe that microexons are frequently misregulated in the brains of autistic individuals, and that this misregulation is linked to the reduced expression of the neural-specific Ser/Arg-related splicing factor of 100 kDa, nSR100/SRRM4. Collectively, our results reveal that alternative microexons represent the most highly conserved component of developmental AS regulation identified to date, and that they function in domain

surface "microsurgery" to control interaction networks associated with neurogenesis. Microexons thus represent a new landscape for investigating the molecular consequences of AS (mis) regulation in nervous system development and ASD.

RESULTS

Global Features of Neural-Regulated AS
An RNA-seq analysis pipeline was developed to detect and quantify all AS event classes involving all hypothetically possible splice junctions formed by the usage of annotated and unannotated splice sites, including those that demarcate microexons. By applying this pipeline to more than 50 diverse cell and tissue types, each from human and mouse (Table S1 available online), we identified ~2,500 neural-regulated AS events in each species (Figure 1A and Table S2; Extended Experimental Procedures).

Nearly half of the neural-regulated AS events, including alternative retained introns, are predicted to generate protein isoforms when the alternative sequence is both included and skipped. In contrast, only ~20% of AS events not subject to neural regulation (hereafter "non-neural" events) have the potential to generate alternative protein isoforms (Figure 1B; $p = 2.7 \times 10^{-248}$, proportion test). Gene Ontology (GO) analysis shows that genes with neural-regulated AS events predicted to generate alternative protein isoforms form highly interconnected networks based on functions associated with neuronal biology, signaling pathways, structural components of the cytoskeleton, and the plasma membrane (Figure 1C). Consistent with previous results (Fagnani et al., 2007; Pan et al., 2004), there is little overlap (8.5%) between genes with neural-regulated AS and mRNA expression, although these subsets of genes are highly enriched in overlapping GO terms (40% in common; Figure S1). These data reveal the largest program of neural-regulated AS events defined to date, and that this program is associated with a broader range of functional processes and pathways linked to nervous system biology than previously detected (Boutz et al., 2007; Fagnani et al., 2007; Ule et al., 2005).

Highly Conserved Microexons Are Frequently Neuron Specific
Further analysis of the neural-regulated AS program revealed a striking inverse relationship between the length of an alternative exon and its propensity to be specifically included in neural tissues. Increased neural-specific inclusion was detected for the majority of microexons (length $\leq$ 27 nt, Figure 2A); 60.7% of alternative microexons show increased neural "percent spliced in" (PSI) (ΔPSI > 15) versus 9.5% of longer (average ~135 nt) alternative exons ($p = 1.9 \times 10^{-220}$, proportion test). This trend extends to microexons as short as 3 nt. RT-PCR validation experiments confirmed the RNA-seq-detected regulatory profiles and inclusion levels of all (10/10) microexons analyzed across ten diverse tissues ($R^2 = 0.92$, n = 107; Figure S2A). To further investigate the cell- and tissue-type specificity of microexon regulation, we used RNA-seq data (Sofueva et al., 2013; Zhang et al., 2013, 2014) to compare their inclusion levels in major glial cell types (astrocytes, microglia, and oligodendrocytes), in isolated neurons, and in muscle cells and tissues. Although up to ~20% of the detected neural-regulated microexons showed
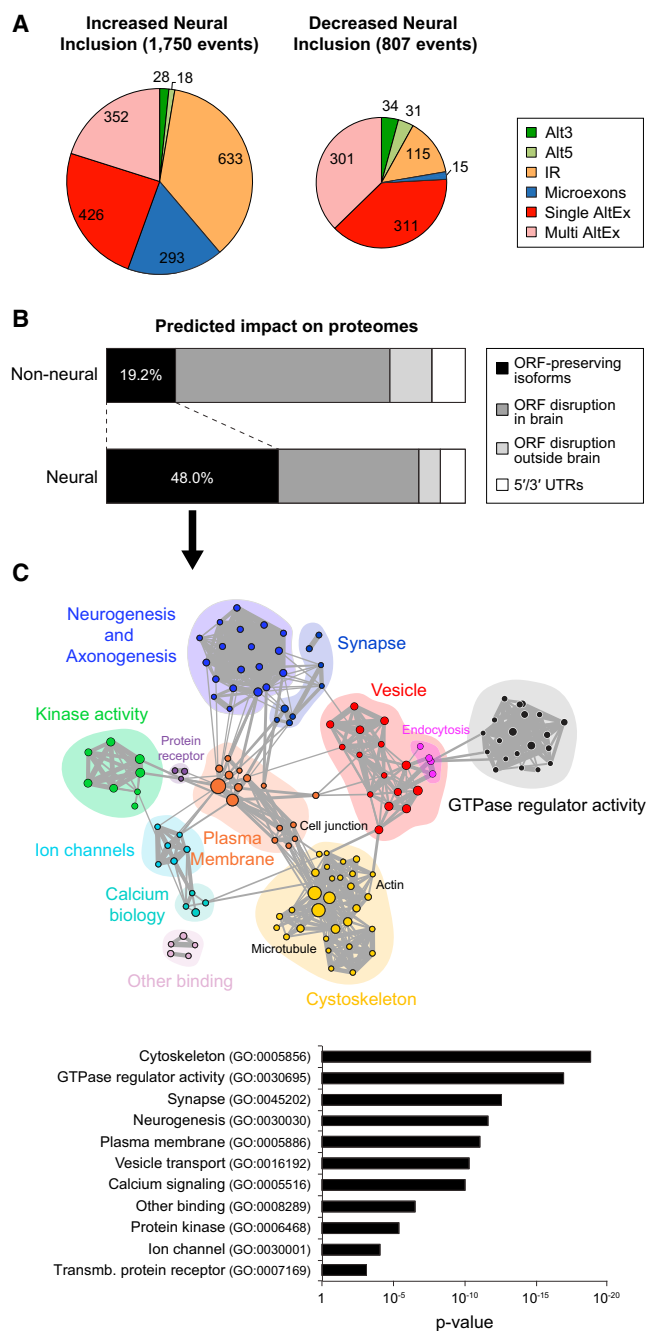
Figure 1. An Extensive Program of Neural-Regulated AS

(A) Distribution by type of human AS events with increased/decreased neural inclusion of the alternative sequence. Alt3/5, alternative splice-site acceptor/donor selection; IR, intron retention; Microexons, 3–27 nt exons; Single/Multi AltEx, single/multiple cassette exons.

(B) Predicted impact of non-neural and neural-regulated AS events on proteomes. Neural-regulated events are more often predicted to generate isoforms preserving open reading frame (ORF) when the alternative sequence is included and excluded ("ORF-preserving isoforms," black), than to disrupt ORFs (i.e., the exon leads to a frameshift and/or introduces a premature termination codon) specifically in neural samples ("ORF disruption in brain," dark gray) or in non-neural samples ("ORF preservation in brain," light gray). See Extended Experimental Procedures for details.

increased PSIs in one or more glial cell types, and/or in muscle, compared to other non-neural tissues, the vast majority (>90%) of neural-regulated microexons displayed highest PSIs in neurons compared to all other cell and tissue types analyzed (Figures S2B–S2D and Extended Experimental Procedures). These results indicate that tissue-regulated microexons are predominantly neuronal specific.

Relative to longer alternative exons, microexons, in particular those that are 3–15 nt long and neural-specifically included, are strongly enriched in multiple features indicative of functionally important AS. They are highly enriched for lengths that are multiples of 3 nt (Figure 2B), and a significantly larger fraction are predicted to generate alternative protein isoforms upon inclusion and exclusion, compared with longer neural exons (Figure 2C; $p < 10^{-10}$, proportion test). They are also significantly more often conserved at the levels of genomic sequence, detection in alternatively spliced transcripts, and neural-differential regulation (Figures 2D and S2E, neural-regulated exons; $p < 0.001$ for all pairwise comparisons, proportion tests). Similar results were obtained when comparing neural-regulated microexons and longer exons that have matching distributions of neural versus non-neural ΔPSI values (data not shown). Of 308 neural-regulated microexons in human, 225 (73.5%) are neural-differentially spliced in mouse, compared to only 527 of 1,390 (37.9%) longer neural-regulated exons. Remarkably, although microexons represent only ∼1% of all AS events, they comprise approximately one-third of all neural-regulated AS events conserved between human and mouse that are predicted to generate alternative protein isoforms (Figure S2F). Moreover, of ∼150 analyzed mammalian, neural-regulated, 3–15 nt microexons, at least 55 are deeply conserved in vertebrate species spanning 400–450 million years of evolution, from zebrafish and/or shark to human (Table S3). This is in marked contrast to the generally low degree of evolutionary conservation of other types of AS across vertebrate species (Barbosa-Morais et al., 2012; Braunschweig et al., 2014; Merkin et al., 2012). Furthermore, comparable numbers of alternative microexons were detected in all analyzed vertebrate species, the majority of which are also strongly neural-specifically included (Figure 2E; Extended Experimental Procedures for details). Consistent with their striking regulatory conservation, sequences overlapping microexons, including both the upstream and downstream flanking intronic regions, are more highly conserved than sequences surrounding longer alternative exons (Figures 2F and S2G), including longer exons with a similar distribution of neural versus non-neural ΔPSI values (Figures S2H and S2I; data not shown).

Dynamic Regulation of Microexons during Neuronal Differentiation

To further investigate the functional significance of neural-regulated microexons, we used RNA-seq data to analyze their

(C) Enrichment map for GO and KEGG categories in genes with neural-regulated AS that are predicted to generate alternative protein isoforms (top) and representative GO terms and their associated enrichment p value for each subnetwork (bottom). The node size is proportional to the number of genes associated with the GO category and the width of the edges to the number of genes shared between GO categories.
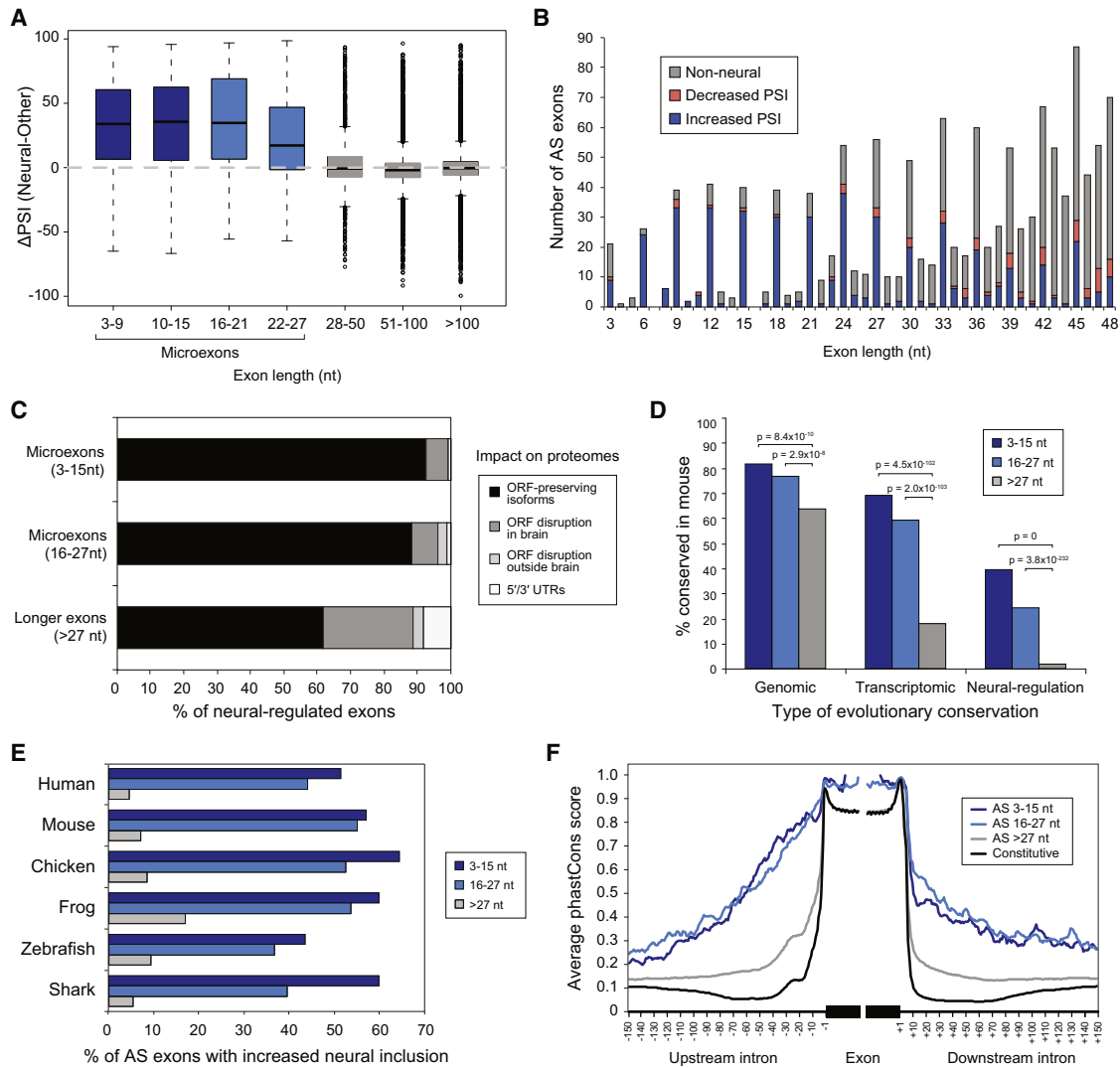
Figure 2. A Landscape of Highly Conserved Neural Microexons

(A) Difference in exon inclusion level (ΔPSI) between the average PSIs for neural samples and non-neural samples (y axis) for bins of increasing exon lengths (x axis). Microexons are defined as exons with lengths of 3–27 nt. Restricting the analysis to alternative exons with a PSI range across samples of >50 showed a similar pattern (data not shown).

(B) Number of exons by length whose inclusion levels are higher (blue), lower (red), or not different (gray) in neural compared to non-neural samples. Short exons tend to be multiple of 3 nt and have higher inclusion in neural samples.

(C) Percent of neural-regulated microexons (of lengths of 3–15 and 16–27 nt) and longer exons that are predicted to generate alternative ORF-preserving isoforms (black), disrupt the ORF in/outside neural tissues (dark/light gray), or overlap noncoding sequences (white).

(D) Higher evolutionary conservation of alternative microexons compared to longer alternative exons at the genomic, transcriptomic (i.e., whether the exon is alternatively spliced in both species), and neural-regulatory levels. y axis shows the percent of conservation at each specific level between human and mouse. p values correspond to two-sided proportion tests.

(E) Percent of alternative microexons and longer exons that are detected as neural-regulated (average absolute ΔPSI > 25) in each vertebrate species.

(F) Alternative 3–15 and 16–27 nt microexons show higher average phastCons scores at their intronic boundaries than longer alternative and constitutive exons. See also Figure S2.

regulation across six time points of differentiation of mouse embryonic stem cells (ESCs) into cortical glutamatergic neurons (Figure 3). Remarkably, of 219 neural-regulated microexons with sufficient read coverage across time points, 151 (69%) displayed a PSI switch ≥50 between ESCs and mature neurons, and 65 (30%) a switch of ≥90 (Figure 3). Unsupervised hierarchi-cal clustering of PSI changes between consecutive time points (transitions T1 to T5) revealed several temporally distinct regula-tory patterns (Figure 3A). Most microexons show sharp PSI switches at late (T3 to T5) transitions during differentiation. These stages correspond to maturing postmitotic neurons when pan-neuronal markers are already expressed and are subsequent

to the expression of most neurogenic transcription factors (Figure S3A). This pattern of late activation (Figure S3B) suggests enrichment for important functions for microexons in terminal neurogenesis (Figure 1C). Despite the small number of genes representing clusters of kinetically distinct sets of regulated microexons, each cluster revealed significant enrichment of specific GO terms including "regulation of GTPase activity" (Cluster I), "glutamate receptor binding," and "actin cytoskeleton organization" (Cluster V) (Table S4). These observations indicate that the dynamic switch-like regulation of microexons is intimately associated with the maturation of neurons.

The Neural-Specific Splicing Factor nSR100/SRRM4 Regulates Most Neural Microexons

Among several analyzed splicing regulators (Extended Experimental Procedures), knockdown and overexpression of nSR100 had the strongest effect on microexon regulation, with more than half of the profiled microexons displaying a pronounced change in inclusion level compared to controls (Figures 4A and S4A–S4H). Moreover, an analysis of RNA-seq data from different neural cell types (Zhang et al., 2014) revealed that nSR100 has the strongest neuronal-specific expression relative to the other splicing regulators (Figure S4I and data not shown), which is also consistent with its immunohistochemical detection in neurons but not glia (Calarco et al., 2009). Recently, we have shown that nSR100 promotes the inclusion of a subset of (longer) neural exons via binding to intronic UGC motifs proximal to suboptimal 3′ splice sites (Raj et al., 2014). Consistent with these results, and supporting a direct role for nSR100 in microexon regulation, RNA sequence tags crosslinked to nSR100 in vivo are also highly enriched in intronic sequences containing UGC motifs, located adjacent to the 3′ splice sites of nSR100-regulated microexons (Figures 4B and 4C; p < 0.0001 for all comparisons; Wilcoxon rank-sum test). We additionally observe that, relative to longer exons, neural-regulated microexons are associated with weak 3′ splice sites and strong 5′ splice sites (Figure S4J). nSR100 thus has a direct and extensive role in the regulation of the neural microexon program.

Distinct Protein-Regulatory Properties of Microexons

Neural-regulated microexons, in particular those that are 3–15 nt long, possess multiple properties that distinguish them from longer neural-regulated exons (Figures 5 and S5). A significantly smaller fraction overlap predicted disordered amino acid residues (Figures 5A and S5A–S5D; p < 1.3 × 10^{-4}; three-way Fisher's exact tests), whereas a significantly higher fraction overlap modular protein domains (Figures 5B and S5E; ∼2-fold increase, p = 1.0 × 10^{-54}; proportion test). In contrast, microexon residues overlapping protein domains are significantly more often surface accessible and enriched in charged residues (Figures 5C, 5D, and S5F–S5I; p < 10^{-7} for all comparisons; proportion test) than are residues overlapping longer neural or non-neural exons. Moreover, when not overlapping protein domains, microexons are significantly more often located immediately adjacent (i.e., within 5 amino acids) to folded protein domains (Figures 5E, S5J, and S5K). These results suggest that a common function of microexons may be to modulate the activity of overlapping or adjacent protein domains. Supporting this view,
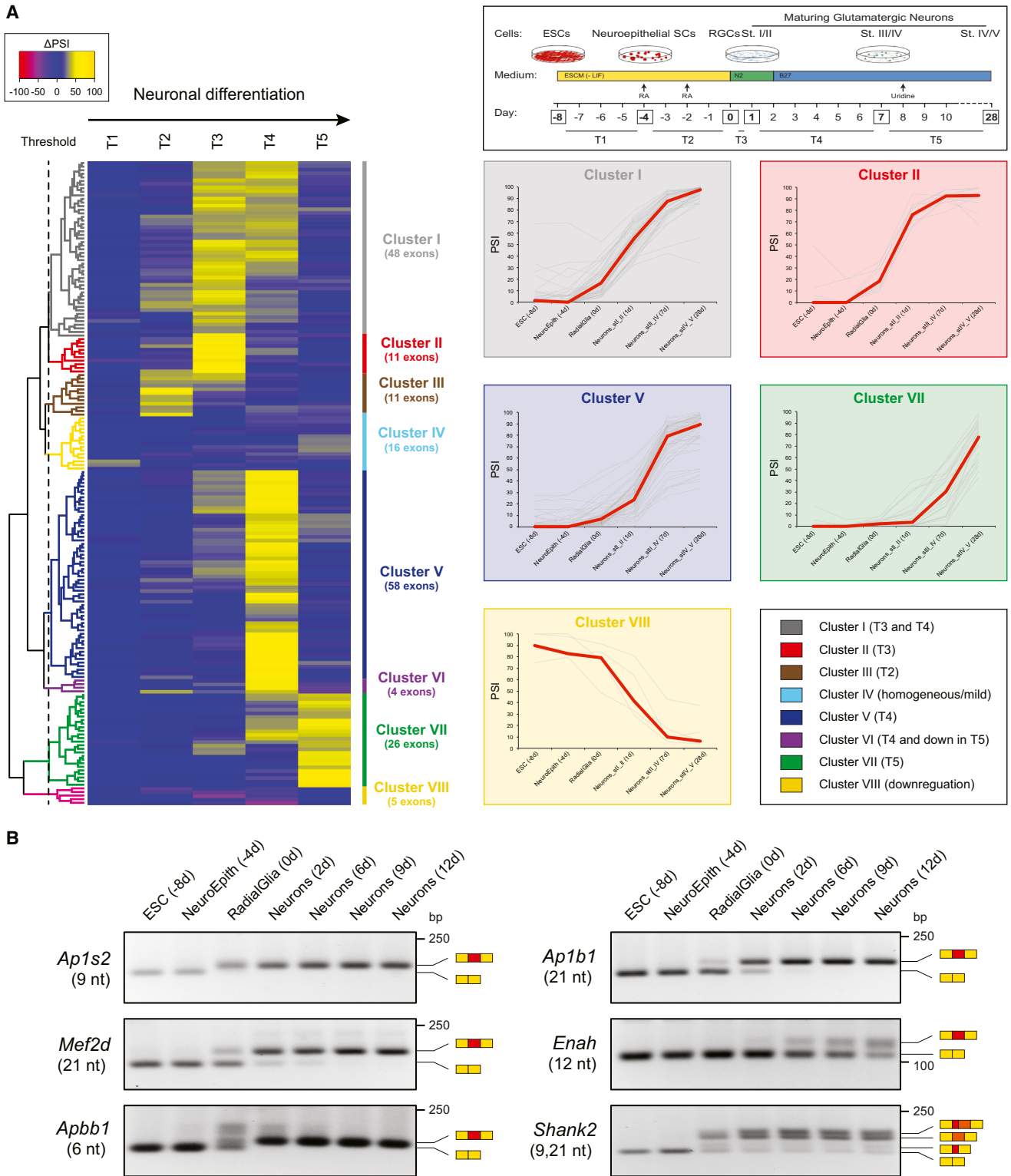
among 49 available and modeled by homology tertiary protein structures containing microexons, the corresponding residues are largely surface accessible and unlikely to significantly affect the folding of the overlapping or adjacent protein domains (Figure S6A; Extended Experimental Procedures).
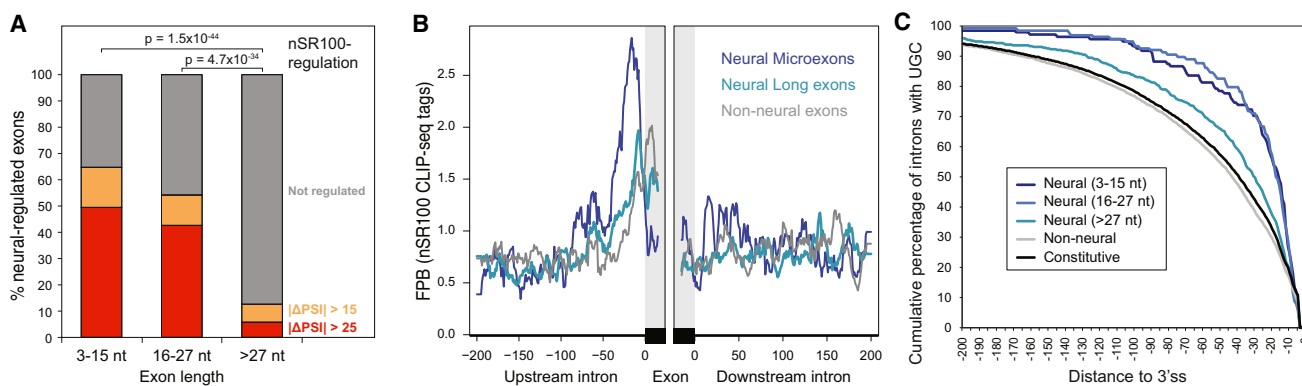
Microexons Modulate the Function of Interaction Domains

Neural-regulated microexons are significantly enriched in domains that function in peptide and lipid-binding interactions (Figures 5F and S5L; p = 1.7 × 10^{-6}; proportion test). Overall, genes with microexons are highly enriched in modular domains involved in cellular signaling, such as SH3 and PH domains (Figure S5M). Conversely, unlike longer neural exons (Buljan et al., 2012; Ellis et al., 2012), they are depleted of linear binding motifs (Figures 5G and S5N; p < 0.005; proportion tests for all comparisons). Moreover, proteins containing microexons are significantly more often central in protein-protein interaction networks and detected in stable protein complexes compared to proteins with other types of alternative exons (Figures 5H, S5O, and S5P; p ≤ 0.004 for all comparisons; Wilcoxon rank-sum test). Taken together with the data in Figure 1, these results suggest that microexons may often regulate interaction domains to facilitate the remodeling of protein-interaction networks associated with signaling and other aspects of neuronal maturation and function.

To test this hypothesis, we employed luminescence-based mammalian interactome mapping (LUMIER; Barrios-Rodiles et al., 2005; Ellis et al., 2012) and coimmunoprecipitation-western blot assays to investigate whether the insertion of a highly conserved, neural-regulated 6 nt microexon in the nuclear adaptor Apbb1 affects its known interactions with the histone acetyltransferase Kat5/Tip60 and amyloid precursor protein App (Figures 6A–6D). Previous genetic and functional studies have revealed multiple functions for the Apbb1-Kat5 complex (Cao and Sudhoff, 2001; Stante et al., 2009), and that the loss of Kat5 activity is associated with developmental defects that impact learning and memory (Pirooznia et al., 2012; Wang et al., 2004, 2009) (see Discussion). Apbb1 contains two phosphotyrosine-binding domains, PTB1 and PTB2, which bind Kat5 and App, respectively (Cao and Sudhoff, 2001). Exemplifying the distinct protein features of neural microexons described above (Figure 5), the Apbb1 microexon adds two charged residues (Arg and Glu) to the PTB1 domain near its predicted interaction surface (Figures 6A and 6B; Extended Experimental Procedures). LUMIER and coimmunoprecipitation-western analysis reveal that inclusion of the microexon significantly enhances the interaction with Kat5, whereas there is little to no effect on the interaction with App (Figures 6C, 6D, S6B, and S6C). Substitution of both microexon residues with alanine also enhanced the Kat5 interaction, although to a lesser extent than the presence of Arg and Glu (Figure 6C). This suggests that the primary function of this microexon is to extend the interface with which Apbb1 binds its partner proteins.

We also examined the function of a 9 nt microexon in the AP1S2 subunit of the adaptor-related protein complex 1 (AP1). The AP1 complex functions in the intracellular transport of cargo proteins between the trans-Golgi apparatus and endosomes by linking clathrin to the cargo proteins during vesicle membrane

Figure 3. Switch-like Regulation of Microexons during Neuronal Differentiation

(A) Heatmap of PSI changes (ΔPSIs) between time points during differentiation of ESCs to glutamatergic neurons in vitro (Hubbard et al., 2013). Yellow/pink indicate increased/decreased PSI at a given transition (T1 to T5). Unsupervised clustering detects eight clusters of exons based on their dynamic PSI regulation

(legend continued on next page)

Figure 4. nSR100 Is a Positive, Direct Regulator of Most Microexons

(A) Percent of neural-regulated exons within each length class that are affected by nSR100 expression in human 293T kidney cells (absolute ΔPSI > 15 [orange] or absolute ΔPSI > 25 [red]). p values correspond to two-sided proportion tests of affected versus nonaffected events.

(B) Average normalized density of nSR100-crosslinked sites in 200 nt windows encompassing neural-regulated exons of different length classes. FPB, fragments per billion.

(C) Cumulative distribution plots indicating the position of the first UGC motif within 200 nt upstream of neural-regulated microexons and longer exons, as well as non-neural and constitutive exons. p < 0.0001 for all comparisons against microexons, Wilcoxon rank-sum test.

See also Figure S4.

formation (Kirchhausen, 2000) and is important for the somato-dendritic transport of proteins required for neuronal polarity (Farías et al., 2012). Interestingly, mutations in AP1S2 have been previously implicated in phenotypic features associated with ASD and X-linked mental retardation (Borck et al., 2008; Tarpey et al., 2006). Coimmunoprecipitation-western analyses reveal that the microexon in AP1S2 strongly promotes its interaction with another AP1 subunit, AP1B1 (Figures 6E and S6D). This observation thus provides additional evidence supporting an important role for microexons in the control of protein interactions that function in neurons.

Microexons Are Misregulated in Individuals with ASD

The properties of microexons described above suggest that their misregulation could be associated with neurological disorders. To investigate this possibility, we analyzed RNA-seq data from the superior temporal gyrus (Brodmann areas ba41/42/22) of postmortem samples from individuals with ASD and control subjects, matched for age, gender, and other variables (Experimental Procedures). These samples were stratified based on the strength of an ASD-associated gene-expression signature (Voineagu et al., 2011), and subsets of 12 ASD samples with the strongest ASD-associated differential gene-expression signatures and 12 controls were selected for further analysis. Remarkably, within these samples, 126 of 504 (30%) detected alternative microexons display a mean ΔPSI > 10 between ASD and control subjects (Figure 7A); of these, 113 (90%) also display neural-differential regulation. By contrast, only 825 of 15,405 (5.4%) longer (i.e., >27 nt) exons show such misregula-

tion (Figure 7A); of these, 285 (35%) correspond to neural-regulated exons. Significant enrichment for misregulation among microexons compared to longer exons was also observed when restricting the analysis to neural-regulated exons, including subsets of neural-regulated microexons and longer exons with similar distributions of neural versus non-neural ΔPSI values (Figure S7A; p < 2 × 10^{-4}; proportion test; data not shown). Similar results were observed when analyzing data from a different brain region (Brodmann area ba9) from the same individuals (data not shown). RT-PCR experiments on a representative subset of profiled tissues confirmed increased misregulation of microexons in autistic versus control brain samples (Figure S7B). Analysis of the proportions of microexons displaying coincident misregulation revealed that the vast majority (81.3%) have a ΔPSI > 10 in at least half of the ASD-stratified brain samples (Figure S7C). However, only 26.9% (32/119) of the genes containing misregulated microexons overlapped with the 2,519 genes with significant ASD-associated misregulation at the level of gene expression. This reveals that largely distinct subsets of genes are misregulated at the levels of expression and microexon splicing in the analyzed ASD subjects. In contrast, a comparison of autistic subjects that possessed a weaker ASD-related differential gene-expression signature did not reveal significant misregulation of microexons or of longer exons (data not shown). These data reveal frequent misregulation of microexon splicing in the brain cortices of some individuals with ASD.

Consistent with a widespread and important role for nSR100 in the regulation of microexons (Figure 4), nSR100 mRNA

(clusters I–VIII, legend). Right, top: scheme of the neuronal differentiation assay, time points of sample collection and analyzed transitions. Right, bottom: PSIs for each microexons (gray lines) in five selected clusters; red lines show the median for the cluster at each time point.

(B) Representative RT-PCR assays monitoring AS patterns of microexons during neuronal differentiation in Ap1s2 (9 nt), Mef2d (21 nt), Apbb1 (6 nt), Ap1b1 (21 nt), Enah (12 nt), and Shank2 (9 and 21 nt).

See also Figure S3.
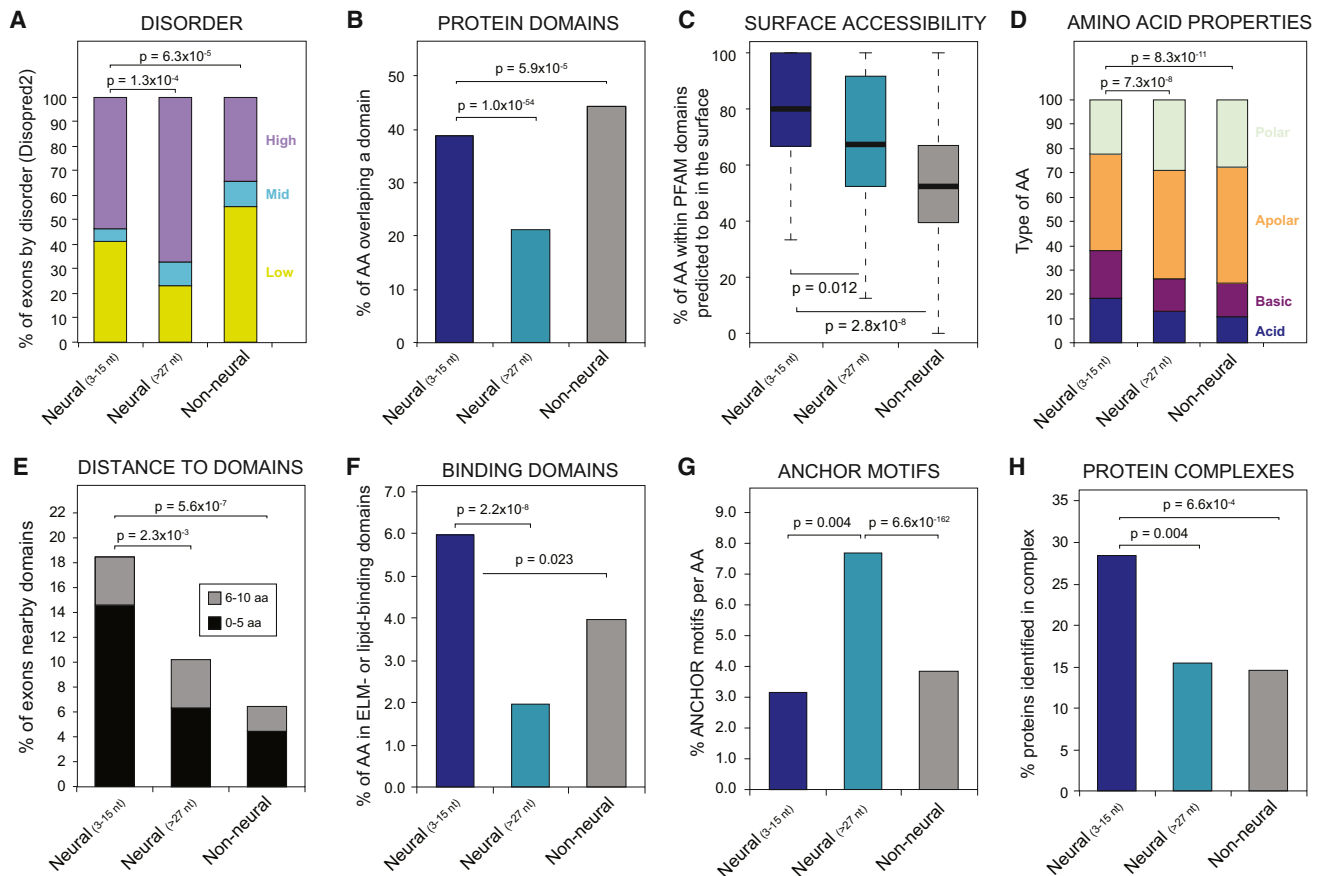
Figure 5. Microexons Possess Distinct Protein-Coding Features

For each analysis, values are shown for neural-regulated, 3–15 nt microexons and longer (>27 nt) exons, as well as non-neural AS exons (see Figure S5 for other types of exons).

(A) Percent of exons with a high average (>0.67), mid-range (0.33 to 0.67), and low disorder rate (<0.33).

(B) Fraction of amino acids (AA) that overlap a PFAM protein domain.

(C) Percent of AA within PFAM domains predicted to be on the protein surface.

(D) Percent of AA types based on their properties; p values correspond to the comparison of charged (acid and basic) versus uncharged (polar and apolar) AAs.

(E) Percent of exons that are adjacent to a domain (within 0–5 [black] or 6–10 AAs [gray]); p values correspond to the comparison of exons within 0–5 AAs.

(F) Percent of residues overlapping PFAM domains involved in linear motif or lipid binding.

(G) Percent of residues overlapping binding motifs predicted by ANCHOR.

(H) Percent of exons with proteins identified as belonging to one or more protein complexes (data from Havugimana et al., 2012).

All p values correspond to proportion tests except for (A) (three-way Fisher's test) and (C) (Wilcoxon rank-sum test). See also Figure S5.

expression is, on average, significantly downregulated in the brains of the analyzed ASD versus control subjects and to an even greater extent in brain samples with the strongest ASD-associated signature compared to the controls (~10%, p = 0.014, FDR < 0.1, Figure 7B and data not shown). These differences were confirmed by qRT-PCR assays for a representative subset of individuals (p < 2.8 × 10^{-4} for all normalizations; two-sided t test; Figure S7D). Moreover, relative to other exons, nSR100-dependent microexons are significantly more often misregulated in brain tissues from ASD compared to control subjects (Figure 7C; p < 0.01 for all comparisons; proportion test). Notably, we also observe significantly higher correlations between microexon inclusion and nSR100 mRNA expression levels across the stratified ASD samples and controls for those microexons regulated by nSR100 relative to those microexons that are

not regulated by this factor (Figure 7D; p = 1.4 × 10^{-7}; Wilcoxon rank-sum test).

A GO analysis of genes with ASD-associated misregulation of microexons reveals significant enrichment of terms related to axonogenesis and synapse biology (Figure 7E), processes that have been previously implicated in autism (Gilman et al., 2011; Parikshak et al., 2013; Voineagu et al., 2011). Many of the corresponding genes act in common pathways and/or physically interact through protein-protein interactions (Figure 7F). Moreover, misregulated microexons are also significantly enriched in genes that have been genetically linked to ASD (p < 0.0005; Fisher's exact test), including many relatively well-established examples such as *DNTA, ANK2, ROBO1, SHANK2,* and *AP1S2.* Other genes with misregulated microexons have been linked to learning or intellectual disability (e.g., *APBB1,*
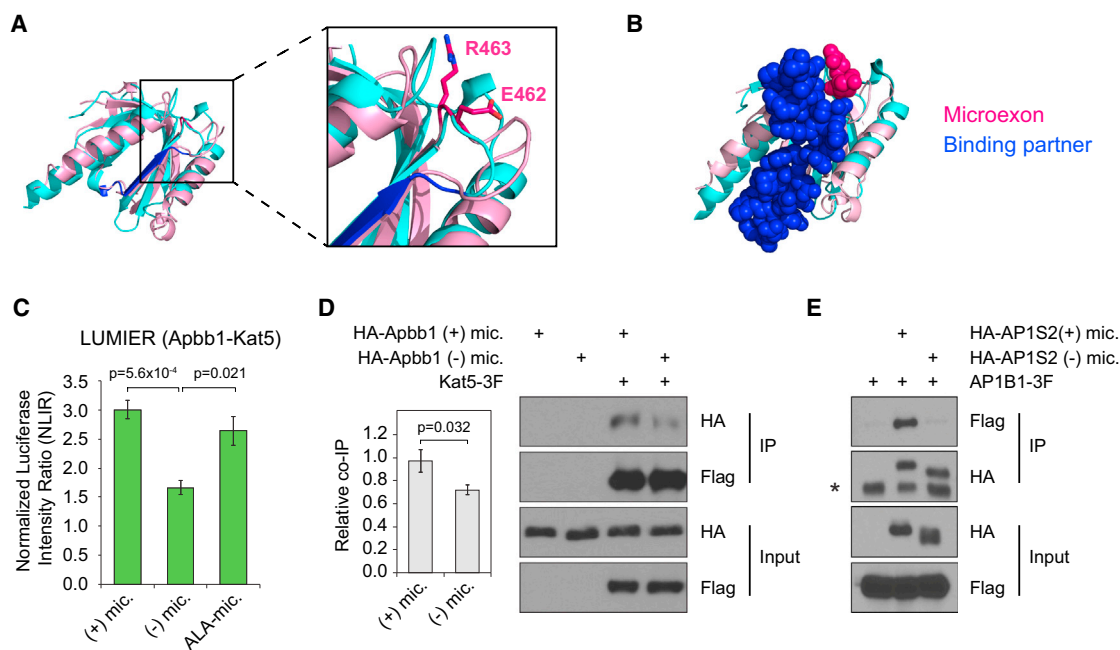
Figure 6. Microexons Regulate Protein-Protein Interactions

(A) Structural alignment of APBB1-PTB1 (pink) and APBB1-PTB2 (cyan) domains. Residues located at the protein-binding interface of APBB1-PTB2 are shown in blue. Inset shows the microexon residues in APBB1-PTB1 (E462-R463).

(B) Upon superimposition of APBB1-PTB1 (pink) and APBB1-PTB2 (cyan) domains, the microexon (magenta) is located close to the APBB1-PTB2-binding partner (APP protein fragment, blue), suggesting that the microexon in PTB1 may affect protein binding.

(C) Quantification of LUMIER-normalized luciferase intensity ratio (NLIR) values for RL-tagged Apbb1, with or without the microexon, or with a mutated version consisting of two alanine substitutions (ALA-mic.), coimmunoprecipitated with 3Flag-tagged Kat5.

(D and E) 293T cells were transfected HA-tagged Apbb1 (D) or AP1S2 (E) constructs, with or without the respective microexon, together with 3Flag-tagged Kat5 (D) or AP1B1 (E), as indicated. Immunoprecipitation was performed with anti-Flag (D) or anti-HA (E) antibody, and the immunoprecipitates were blotted with anti-HA or anti-Flag antibody, as indicated. Results shown in (E) were confirmed in a biological replicate experiment (Figure S6D).

p values in (C) and (D) correspond to t tests for four and three replicates, respectively; error bars indicate SEM. Asterisk in (E) indicates a band corresponding to the light chain of the HA antibody.


TRAPPC9, and *RAB3GAP1*). In this regard, it is interesting to note that the microexons we have analyzed in APBB1 and AP1S2 are significantly misregulated in the brain samples from ASD subjects (p < 0.05; Wilcoxon rank-sum test; Figure S7E). Taken together with data in Figures 5 and 6, the results suggest that the misregulation of microexons, as well as of longer alternative exons (Corominas et al., 2014; Voineagu et al., 2011), may impact protein-interaction networks that are required for normal neuronal development and synaptic function. Disruption of microexon-regulated protein-interaction networks is therefore a potentially important mechanism underlying ASD and likely other neurodevelopmental disorders.

DISCUSSION

In this study, we show that alternative microexons display the highest degrees of genomic sequence conservation, tissue-specific regulatory conservation, and frame-preservation potential, relative to all other classes of AS detected to date in vertebrate species. Unlike longer neural-regulated exons, neural microexons are significantly enriched in surface-accessible, charged amino acids that overlap or lie in close proximity to protein domains, including those that bind linear motifs. Together with their

remarkably dynamic regulation, these observations suggest that microexons contribute important and complementary roles to longer neural exons in the remodeling of protein-interaction networks that operate during neuronal maturation.

Most microexons display high inclusion at late stages of neuronal differentiation in genes (e.g., *Src* [Black, 1991], *Bin1*, *Agrn*, *Dock9*, *Shank2*, and *Robo1*) associated with axonogenesis and the formation and function of synapses. Supporting such functions, an alternative microexon overlapping the SH3A domain of Intersectin 1 (Itsn1) has been reported to promote an interaction with Dynamin 1 and was proposed to modulate roles of Itsn1 in endocytosis, cell signaling, and/or actin-cytoskeleton dynamics (Dergai et al., 2010). A neural-specific microexon in Protrudin/Zfyve27 was recently shown to increase its interaction with the vesicle-associated membrane protein-associated protein (VAP) and to promote neurite outgrowth (Ohnishi et al., 2014). Similarly, in the present study, we show that a 6 nt neural microexon in Apbb1/Fe65 promotes an interaction with Kat5/Tip60. Apbb1 is an adaptor protein that functions in neurite outgrowth (Cheung et al., 2014; Ikin et al., 2007) and synaptic plasticity (Sabo et al., 2003), processes that have been linked to neurological disorders including ASD (Hussman et al., 2011). Consistent with these findings, we have previously shown
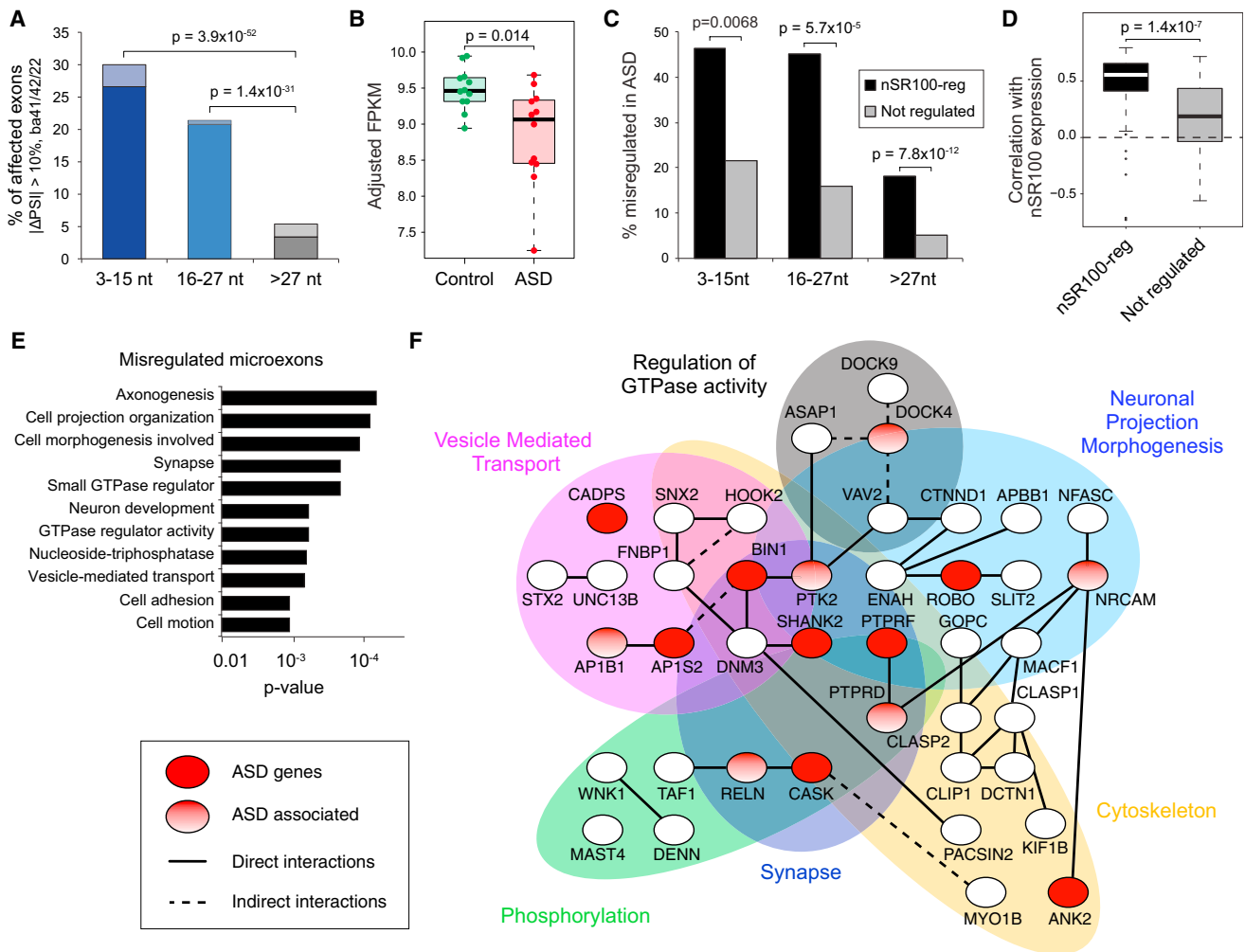
Figure 7. Microexons Are Often Misregulated in ASD

(A) Percent of alternative exons of each length class that are misregulated in ASD (absolute ΔPSI > 10 between PSI-averaged ASD and control groups in ba41/42/22 brain regions). Dark shading, lower inclusion in ASD; light shading, higher inclusion in ASD; p values correspond to proportion tests.

(B) Expression of nSR100 across the 12 control and 12 ASD individuals. Adjusted FPKMs were calculated using a regression analysis that accounts for variation derived from differences in RNA integrity, brain sample batch, sequencing depth, and 5′–3′ bias in measurements of gene-level FPKM values.

(C) Percent of exons within each length class misregulated in autistic compared to control brains (average absolute ΔPSI > 10) for nSR100-regulated (ΔPSI > 25 in the nSR100-overexpressing compared to control 293T cells) and non-nSR100-regulated (absolute ΔPSI < 5) exons.

(D) Distribution of correlation coefficients between PSIs and nSR100 expression values across stratified ASD and control samples for microexons that are (n = 59) or are not (n = 69) regulated by nSR100. Only microexons with sufficient read coverage to derive accurate PSI quantifications in at least 9 ASD and 9 control ba41/42/22 samples were included. p value correspond to Wilcoxon rank-sum test.

(E) GO categories significantly enriched in genes with microexons that are misregulated in ASD.

(F) A protein-protein interaction network involving genes with ASD misregulated microexons (ΔPSI > 10) in ba41/42/22 brain regions. Genes with major effect mutations, and smaller effect risk genes, are indicated in red and shaded ovals, respectively. Genes grouped by functional category are indicated.

See also Figure S7.

that nSR100 promotes neurite outgrowth (Calarco et al., 2009). In the present study, we further demonstrate that it controls the switch-like regulation of most neural microexons, and that its reduced expression is linked to the altered splicing of microexons in the brains of subjects with ASD.

Many of the conserved, neural-regulated microexons identified in this study are misregulated in ASD individuals, including the microexon in AP1S2 that strongly promotes an interaction with the AP1B1 subunit of the AP1 intracellular transport com-

plex. Intriguingly, several other genes containing microexons are genetically linked to ASD, intellectual disability, and/or functions in memory and learning (see Results). Another link to ASD is the observation that nSR100 is strongly coexpressed in the developing human brain in a gene network module, M2, which is enriched for rare de novo ASD-associated mutations (Parikshak et al., 2013). Furthermore, additional genes containing microexons may have as yet undiscovered roles in ASD and or other neuropsychiatric disorders. For example, the microexon

in APBB1 is also significantly misregulated in brain tissues from ASD subjects (Figures S7B and S7E). It is possible that the misregulation of microexons, at least in part through altered expression of nSR100, perturbs protein-interaction networks required for proper neuronal maturation and function, thus contributing to ASD as well as other neurodevelopmental disorders. Consistent with this view, recent reports have begun to link individual microexons with neurodevelopmental disorders, including ASD (Zhu et al., 2014), schizophrenia (Ovadia and Shifman, 2011), and epilepsy (Rusconi et al., 2014). The discovery and characterization of widespread, neural-regulated microexons in the present study thus enable a systematic investigation of new and highly conserved mechanisms controlling protein-interaction networks associated with vertebrate nervous system development and neurological disorders.

EXPERIMENTAL PROCEDURES

RNA-Seq Data and Genomes

Unless stated otherwise, RNA-seq data were generated from poly(A)$^+$ RNA (Table S1). Analyses used the following genome releases: *Homo sapiens*, hg19; *Mus musculus*, mm9; *Gallus gallus*, galGal3; *Xenopus tropicalis*, xenTro3; *Danio rerio*, danRer7; *Callorhinchus milii*, v1.0.

AS Analysis Pipeline

A multimodule analysis pipeline was developed that uses RNA-seq, expressed sequence tag (EST), and cDNA data, as well as gene annotations and evolutionary conservation, to assemble libraries of exon-exon junctions (EEJs) for subsequent read alignment to detect and quantify AS events in RNA-seq data. For cassette exons, three complementary modules were developed for assembling EEJs: (1) a "transcript-based module," employing cufflinks (Trapnell et al., 2010) and alignments of ESTs and cDNAs with genomic sequence (Khare et al., 2012); (2) a "splice site-based module," utilizing joining of all hypothetically possible EEJ combinations from annotated and de novo splice sites (Han et al., 2013); and (3) a "microexon module," including de novo searching of pairs of donor and acceptor splice sites in intronic sequence. Alt3 or Alt5 events were quantified based on the fraction of reads supporting the usage of each alternative splice site. Intron retention was analyzed as recently described (Braunschweig et al., 2014). See Extended Experimental Procedures for additional details. All described human microexons and associated features are provided in Tables S5 and S6.

LUMIER Assay

HEK293T cells were transiently transfected using Polyfect (QIAGEN) with *Renilla* luciferase (RL)-tagged Apbb1, with or without inclusion of the microexon, or with a version consisting of two alanine substitutions, together with 3Flag-tagged Kat5. Subsequent steps were performed essentially as described previously (Ellis et al., 2012).

Immunoprecipitation and Immunoblotting

HEK293T cells were transiently transfected using Lipofectamine 2000 (Life Technologies). Cells were lysed in 0.5% TNTE. After preclearing with protein G-Sepharose, lysates were incubated with anti-Flag M2 antibody (Sigma) or anti-Hemagglutinin (HA) antibody (Roche) bound to Protein-G Dynabeads (Life Technologies) for 2 hr at 4°C. Immunoprecipitates were washed five times with 0.1% TNTE, subjected to SDS-PAGE, transferred onto nitrocellulose, and immunoblotted with the anti-HA antibody (Roche) or anti-Flag M2 antibody (Sigma). Detection was achieved using horseradish peroxidase-conjugated rabbit anti-rat (Sigma) or sheep anti-mouse secondary antibodies (GE Healthcare) and chemiluminescence. ImageJ was used for quantification of band intensities.

Analysis of Microexon Regulation

Available RNA-seq data from splicing factor-deficient or -overexpressing systems were used to identify misregulated exons and microexons (see Extended Experimental Procedures). To investigate regulation by nSR100, we used PAR-iCLIP data and motif enrichments analyses, as recently described (Raj et al., 2014).

Comparison of ASD and Control Brain Samples

We analyzed 22 autistic individuals and 20 controls matched by age and gender. Samples from superior temporal gyrus (Brodmann areas ba41/42/22) were dissected, retaining gray matter from all cortical layers, and RNA was isolated using the miRNeasy kit (QIAGEN). Ribosomal RNA was depleted from 2 μg total RNA with the Ribo-Zero Gold kit (Epicenter) and then size-selected with AMPure XP beads (Beckman Coulter). An average of 64 million, 50 bp paired-end reads were generated for each sample (Table S1). The 12 case and 12 control samples with the strongest ASD-associated differential gene-expression signature were selected for downstream analyses (Extended Experimental Procedures for details). Sample selection was independent of any information on splicing changes.

ACCESSION NUMBERS

The BioProject ID for the RNA-seq data reported in this paper is PRJNA268211. The Gene Expression Omnibus (GEO) accession number for the RNA-seq data is GSE64018.

SUPPLEMENTAL INFORMATION

Supplemental Information includes Extended Experimental Procedures, seven figures, and six tables and can be found with this article online at http://dx.doi.org/10.1016/j.cell.2014.11.035.

AUTHOR CONTRIBUTIONS

ACKNOWLEDGMENTS

Chairs Program. B.J.B. holds the Banbury Chair of Medical Research at the University of Toronto.

REFERENCES

Barbosa-Morais, N.L., Irimia, M., Pan, Q., Xiong, H.Y., Gueroussov, S., Lee, L.J., Slobodeniuc, V., Kutter, C., Watt, S., Colak, R., et al. (2012). The evolutionary landscape of alternative splicing in vertebrate species. Science *338*, 1587–1593.

Barrios-Rodiles, M., Brown, K.R., Ozdamar, B., Bose, R., Liu, Z., Donovan, R.S., Shinjo, F., Liu, Y., Dembowy, J., Taylor, I.W., et al. (2005). High-throughput mapping of a dynamic signaling network in mammalian cells. Science *307*, 1621–1625.

Beachy, P.A., Helfand, S.L., and Hogness, D.S. (1985). Segmental distribution of bithorax complex proteins during Drosophila development. Nature *313*, 545–551.

Black, D.L. (1991). Does steric interference between splice sites block the splicing of a short c-src neuron-specific exon in non-neuronal cells? Genes Dev. *5*, 389–402.

Borck, G., Mollà-Herman, A., Boddaert, N., Encha-Razavi, F., Philippe, A., Robel, L., Desguerre, I., Brunelle, F., Benmerah, A., Munnich, A., and Colleaux, L. (2008). Clinical, cellular, and neuropathological consequences of AP1S2 mutations: further delineation of a recognizable X-linked mental retardation syndrome. Hum. Mutat. *29*, 966–974.

Boutz, P.L., Stoilov, P., Li, Q., Lin, C.H., Chawla, G., Ostrow, K., Shiue, L., Ares, M.J., Jr., and Black, D.L. (2007). A post-transcriptional regulatory switch in polypyrimidine tract-binding proteins reprograms alternative splicing in developing neurons. Genes Dev. *21*, 1636–1652.

Braunschweig, U., Gueroussov, S., Plocik, A.M., Graveley, B.R., and Blencowe, B.J. (2013). Dynamic integration of splicing within gene regulatory pathways. Cell *152*, 1252–1269.

Braunschweig, U., Barbosa-Morais, N.L., Pan, Q., Nachman, E.N., Alipanahi, B., Gonatopoulos-Pournatzis, T., Frey, B., Irimia, M., and Blencowe, B.J. (2014). Widespread intron retention in mammals functionally tunes transcriptomes. Genome Res. *24*, 1774–1786.

Buljan, M., Chalancon, G., Eustermann, S., Wagner, G.P., Fuxreiter, M., Bateman, A., and Babu, M.M. (2012). Tissue-specific splicing of disordered segments that embed binding motifs rewires protein interaction networks. Mol. Cell *46*, 871–883.

Calarco, J.A., Superina, S., O'Hanlon, D., Gabut, M., Raj, B., Pan, Q., Skalska, U., Clarke, L., Gelinas, D., van der Kooy, D., et al. (2009). Regulation of vertebrate nervous system alternative splicing and development by an SR-related protein. Cell *138*, 898–910.

Calarco, J.A., Zhen, M., and Blencowe, B.J. (2011). Networking in a global world: establishing functional connections between neural splicing regulators and their target transcripts. RNA *17*, 775–791.

Cao, X., and Sudhoff, T.C. (2001). A transcriptionally active complex of APP with Fe65 and histone acetyltransferase Tip60. Science *293*, 115–120.

Cartegni, L., Chew, S.L., and Krainer, A.R. (2002). Listening to silence and understanding nonsense: exonic mutations that affect splicing. Nat. Rev. Genet. *3*, 285–298.

Chen, M., and Manley, J.L. (2009). Mechanisms of alternative splicing regulation: insights from molecular and genomics approaches. Nat. Rev. Mol. Cell Biol. *10*, 741–754.

Cheung, H.N., Dunbar, C., Mórotz, G.M., Cheng, W.H., Chan, H.Y., Miller, C.C., and Lau, K.F. (2014). FE65 interacts with ADP-ribosylation factor 6 to promote neurite outgrowth. FASEB J. *28*, 337–349.

Coleman, K.G., Poole, S.J., Weir, M.P., Soeller, W.C., and Kornberg, T. (1987). The invected gene of Drosophila: sequence analysis and expression studies reveal a close kinship to the engrailed gene. Genes Dev. *1*, 19–28.

Corominas, R., Yang, X., Lin, G.N., Kang, S., Shen, Y., Ghamsari, L., Broly, M., Rodriguez, M., Tam, S., Trigg, S.A., et al. (2014). Protein interaction network of alternatively spliced isoforms from brain links genetic risk factors for autism. Nat. Commun. *5*, 3650.

David, C.J., and Manley, J.L. (2010). Alternative pre-mRNA splicing regulation in cancer: pathways and programs unhinged. Genes Dev. *24*, 2343–2364.

Dergai, M., Tsyba, L., Dergai, O., Zlatskii, I., Skrypkina, I., Kovalenko, V., and Rynditch, A. (2010). Microexon-based regulation of ITSN1 and Src SH3 domains specificity relies on introduction of charged amino acids into the interaction interface. Biochem. Biophys. Res. Commun. *399*, 307–312.

Ellis, J.D., Barrios-Rodiles, M., Colak, R., Irimia, M., Kim, T., Calarco, J.A., Wang, X., Pan, Q., O'Hanlon, D., Kim, P.M., et al. (2012). Tissue-specific alternative splicing remodels protein-protein interaction networks. Mol. Cell *46*, 884–892.

Eom, T., Zhang, C., Wang, H., Lay, K., Fak, J., Noebels, J.L., and Darnell, R.B. (2013). NOVA-dependent regulation of cryptic NMD exons controls synaptic protein levels after seizure. Elife *2*, e00178.

Fagnani, M., Barash, Y., Ip, J.Y., Misquitta, C., Pan, Q., Saltzman, A.L., Shai, O., Lee, L., Rozenhek, A., Mohammad, N., et al. (2007). Functional coordination of alternative splicing in the mammalian central nervous system. Genome Biol. *8*, R108.

Farías, G.G., Cuitino, L., Guo, X., Ren, X., Jarnik, M., Mattera, R., and Bonifacino, J.S. (2012). Signal-mediated, AP-1/clathrin-dependent sorting of transmembrane receptors to the somatodendritic domain of hippocampal neurons. Neuron *75*, 810–823.

Gilman, S.R., Iossifov, I., Levy, D., Ronemus, M., Wigler, M., and Vitkup, D. (2011). Rare de novo variants associated with autism implicate a large functional network of genes involved in formation and function of synapses. Neuron *70*, 898–907.

Han, H., Irimia, M., Ross, P.J., Sung, H.K., Alipanahi, B., David, L., Golipour, A., Gabut, M., Michael, I.P., Nachman, E.N., et al. (2013). MBNL proteins repress ES-cell-specific alternative splicing and reprogramming. Nature *498*, 241–245.

Havugimana, P.C., Hart, G.T., Nepusz, T., Yang, H., Turinsky, A.L., Li, Z., Wang, P.I., Boutz, D.R., Fong, V., Phanse, S., et al. (2012). A census of human soluble protein complexes. Cell *150*, 1068–1081.

Hubbard, K.S., Gut, I.M., Lyman, M.E., and McNutt, P.M. (2013). Longitudinal RNA sequencing of the deep transcriptome during neurogenesis of cortical glutamatergic neurons from murine ESCs. F1000Res *2*, 35. http://dx.doi.org/10.12688/f1000research.2-35.v1.

Hussman, J.P., Chung, R.H., Griswold, A.J., Jaworski, J.M., Salyakina, D., Ma, D., Konidari, I., Whitehead, P.L., Vance, J.M., Martin, E.R., et al. (2011). A noise-reduction GWAS analysis implicates altered regulation of neurite outgrowth and guidance in autism. Mol. Autism *2*, 1.

Ikin, A.F., Sabo, S.L., Lanier, L.M., and Buxbaum, J.D. (2007). A macromolecular complex involving the amyloid precursor protein (APP) and the cytosolic adapter FE65 is a negative regulator of axon branching. Mol. Cell. Neurosci. *35*, 57–63.

Irimia, M., and Blencowe, B.J. (2012). Alternative splicing: decoding an expansive regulatory layer. Curr. Opin. Cell Biol. *24*, 323–332.

Kalsotra, A., and Cooper, T.A. (2011). Functional consequences of developmentally regulated alternative splicing. Nat. Rev. Genet. *12*, 715–729.

Khare, T., Pai, S., Koncevicius, K., Pal, M., Kriukiene, E., Liutkeviciute, Z., Irimia, M., Jia, P., Ptak, C., Xia, M., et al. (2012). 5-hmC in the brain is abundant in synaptic genes and shows differences at the exon-intron boundary. Nat. Struct. Mol. Biol. *19*, 1037–1043.

Kirchhausen, T. (2000). Clathrin. Annu. Rev. Biochem. *69*, 699–727.

Licatalosi, D.D., and Darnell, R.B. (2010). RNA processing and its regulation: global insights into biological networks. Nat. Rev. Genet. *11*, 75–87.

Merkin, J., Russell, C.B., Chen, P., and Burge, C.B. (2012). Evolutionary dynamics of gene and isoform regulation in mammalian tissues. Science *338*, 1593–1599.

Ohnishi, T., Shirane, M., Hashimoto, Y., Saita, S., and Nakayama, K.I. (2014). Identification and characterization of a neuron-specific isoform of protrudin. Genes Cells *19*, 97–111.

Ovadia, G., and Shifman, S. (2011). The genetic variation of RELN expression in schizophrenia and bipolar disorder. PLoS ONE *6*, e19955.

Pan, Q., Shai, O., Misquitta, C., Zhang, W., Saltzman, A.L., Mohammad, N., Babak, T., Siu, H., Hughes, T.R., Morris, Q.D., et al. (2004). Revealing global regulatory features of mammalian alternative splicing using a quantitative microarray platform. Mol. Cell *16*, 929–941.

Pan, Q., Shai, O., Lee, L.J., Frey, B.J., and Blencowe, B.J. (2008). Deep surveying of alternative splicing complexity in the human transcriptome by high-throughput sequencing. Nat. Genet. *40*, 1413–1415.

Parikshak, N.N., Luo, R., Zhang, A., Won, H., Lowe, J.K., Chandran, V., Horvath, S., and Geschwind, D.H. (2013). Integrative functional genomic analyses implicate specific molecular pathways and circuits in autism. Cell *155*, 1008–1021.

Pirooznia, S.K., Sarthi, J., Johnson, A.A., Toth, M.S., Chiu, K., Koduri, S., and Elefant, F. (2012). Tip60 HAT activity mediates APP induced lethality and apoptotic cell death in the CNS of a Drosophila Alzheimer's disease model. PLoS ONE *7*, e41776.

Polymenidou, M., Lagier-Tourenne, C., Hutt, K.R., Bennett, C.F., Cleveland, D.W., and Yeo, G.W. (2012). Misregulated RNA processing in amyotrophic lateral sclerosis. Brain Res. *1462*, 3–15.

Raj, B., Irimia, M., Braunschweig, U., Sterne-Weiler, T., O'Hanlon, D., Lin, Z.Y., Chen, G.I., Easton, L.E., Ule, J., Gingras, A.C., et al. (2014). A global regulatory mechanism for activating an exon network required for neurogenesis. Mol. Cell *56*, 90–103.

Romero, P.R., Zaidi, S., Fang, Y.Y., Uversky, V.N., Radivojac, P., Oldfield, C.J., Cortese, M.S., Sickmeier, M., LeGall, T., Obradovic, Z., and Dunker, A.K. (2006). Alternative splicing in concert with protein intrinsic disorder enables increased functional diversity in multicellular organisms. Proc. Natl. Acad. Sci. USA *103*, 8390–8395.

Rusconi, F., Paganini, L., Braida, D., Ponzoni, L., Toffolo, E., Maroli, A., Landsberger, N., Bedogni, F., Turco, E., Pattini, L., et al. (2014). LSD1 neurospecific alternative splicing controls neuronal excitability in mouse models of epilepsy. Cereb. Cortex. Published online April 15, 2014. http://dx.doi.org/10.1093/cercor/bhu070.

Sabo, S.L., Ikin, A.F., Buxbaum, J.D., and Greengard, P. (2003). The amyloid precursor protein and its regulatory protein, FE65, in growth cones and synapses in vitro and in vivo. J. Neurosci. *23*, 5407–5415.

Sofueva, S., Yaffe, E., Chan, W.C., Georgopoulou, D., Vietri Rudan, M., Mira-Bontenbal, H., Pollard, S.M., Schroth, G.P., Tanay, A., and Hadjur, S. (2013). Cohesin-mediated interactions organize chromosomal domain architecture. EMBO J. *32*, 3119–3129.

Stante, M., Minopoli, G., Passaro, F., Raia, M., Vecchio, L.D., and Russo, T. (2009). Fe65 is required for Tip60-directed histone H4 acetylation at DNA strand breaks. Proc. Natl. Acad. Sci. USA *106*, 5093–5098.

Tarpey, P.S., Stevens, C., Teague, J., Edkins, S., O'Meara, S., Avis, T., Barthorpe, S., Buck, G., Butler, A., Cole, J., et al. (2006). Mutations in the gene encoding the Sigma 2 subunit of the adaptor protein 1 complex, AP1S2, cause X-linked mental retardation. Am. J. Hum. Genet. *79*, 1119–1124.

Trapnell, C., Williams, B.A., Pertea, G., Mortazavi, A., Kwan, G., van Baren, M.J., Salzberg, S.L., Wold, B.J., and Pachter, L. (2010). Transcript assembly and quantification by RNA-Seq reveals unannotated transcripts and isoform switching during cell differentiation. Nat. Biotechnol. *28*, 511–515.

Ule, J., Ule, A., Spencer, J., Williams, A., Hu, J.S., Cline, M., Wang, H., Clark, T., Fraser, C., Ruggiu, M., et al. (2005). Nova regulates brain-specific splicing to shape the synapse. Nat. Genet. *37*, 844–852.

Voineagu, I., Wang, X., Johnston, P., Lowe, J.K., Tian, Y., Horvath, S., Mill, J., Cantor, R.M., Blencowe, B.J., and Geschwind, D.H. (2011). Transcriptomic analysis of autistic brain reveals convergent molecular pathology. Nature *474*, 380–384.

Volfovsky, N., Haas, B.J., and Salzberg, S.L. (2003). Computational discovery of internal micro-exons. Genome Res. *13* (6A), 1216–1221.

Wahl, M.C., Will, C.L., and Lührmann, R. (2009). The spliceosome: design principles of a dynamic RNP machine. Cell *136*, 701–718.

Wang, B., Hu, Q., Hearn, M.G., Shimizu, K., Ware, C.B., Liggitt, D.H., Jin, L.W., Cool, B.H., Storm, D.R., and Martin, G.M. (2004). Isoform-specific knockout of FE65 leads to impaired learning and memory. J. Neurosci. Res. *75*, 12–24.

Wang, E.T., Sandberg, R., Luo, S., Khrebtukova, I., Zhang, L., Mayr, C., Kingsmore, S.F., Schroth, G.P., and Burge, C.B. (2008). Alternative isoform regulation in human tissue transcriptomes. Nature *456*, 470–476.

Wang, Y., Zhang, M., Moon, C., Hu, Q., Wang, B., Martin, G., Sun, Z., and Wang, H. (2009). The APP-interacting protein FE65 is required for hippocampus-dependent learning and long-term potentiation. Learn. Mem. *16*, 537–544.

Weatheritt, R.J., Davey, N.E., and Gibson, T.J. (2012). Linear motifs confer functional diversity onto splice variants. Nucleic Acids Res. *40*, 7123–7131.

Wu, J., Anczuków, O., Krainer, A.R., Zhang, M.Q., and Zhang, C. (2013). OLego: fast and sensitive mapping of spliced mRNA-Seq reads using small seeds. Nucleic Acids Res. *41*, 5149–5163.

Wu, T.D., and Watanabe, C.K. (2005). GMAP: a genomic mapping and alignment program for mRNA and EST sequences. Bioinformatics *21*, 1859–1875.

Zhang, Z., Pinto, A.M., Wan, L., Wang, W., Berg, M.G., Oliva, I., Singh, L.N., Dengler, C., Wei, Z., and Dreyfuss, G. (2013). Dysregulation of synaptogenesis genes antecedes motor neuron pathology in spinal muscular atrophy. Proc. Natl. Acad. Sci. USA *110*, 19348–19353.

Zhang, Y., Chen, K., Sloan, S.A., Bennett, M.L., Scholze, A.R., O'Keeffe, S., Phatnani, H.P., Guarnieri, P., Caneda, C., Ruderisch, N., et al. (2014). An RNA-sequencing transcriptome and splicing database of glia, neurons, and vascular cells of the cerebral cortex. J. Neurosci. *34*, 11929–11947.

Zhu, L., Wang, X., Li, X.L., Towers, A., Cao, X., Wang, P., Bowman, R., Yang, H., Goldstein, J., Li, Y.J., and Jiang, Y.H. (2014). Epigenetic dysregulation of SHANK3 in brain tissues from individuals with autism spectrum disorders. Hum. Mol. Genet. *23*, 1563–1578.